

A novel configuration of gluonic tetraquark state

Chun-Meng Tang¹, Chun-Gui Duan^{2,3 *}, Liang Tang^{1,†} and Cong-Feng Qiao^{4‡}

¹College of Physics and Hebei Key Laboratory of Photophysics Research and Application,

Hebei Normal University, Shijiazhuang 050024, China

²College of Physics and Hebei Advanced Thin Film Laboratory,

Hebei Normal University, Shijiazhuang 050024, China

³ Hebei Key Laboratory of Physics and Energy Technology,

North China Electric Power University, Baoding 071000, China

⁴ School of Physical Sciences, University of Chinese Academy of Sciences, Yuquan Road 19A, Beijing 100049, China

Inspired by the experimental measurement of the charmed hadronic state X(6900), we calculate the mass spectra of tetraquark hybrid states with configuration of $[8_c]_{Q\bar{Q}} \otimes [8_c]_G \otimes [8_c]_{Q\bar{Q}}$ in color, by virtue of QCD sum rules. The two feasible types of currents with quantum numbers $J^{PC} = 0^{++}$ and 0^{-+} are investigated, in which the contributions from operators up to dimension six are taken into account in operator product expansion (OPE). In the end, we find that, in charm sector, the tetracharm hybrid states with quantum number 0^{++} has a mass of about $6.98^{+0.16}_{-0.14}$ GeV, while 0^{-+} state mass is about $7.26^{+0.16}_{-0.15}$ GeV. The results overlap with the experimental observations, suggesting potential tetracharm hybrid interpretations. In bottom sector, calculation shows that the masses of tetrabottom hybrid states with quantum numbers 0^{++} and 0^{-+} are $19.30^{+0.16}_{-0.17}$ GeV and $19.50^{+0.17}_{-0.17}$ GeV, respectively, which are left for future experimental confirmation.

I. INTRODUCTION

In the traditional quark model [1, 2], hadrons are classified into two types: mesons ($q\bar{q}$) and baryons (qqq). However, Quantum Chromodynamics (QCD) [3–5] allows for the existence of exotic hadron states beyond ordinary mesons and baryons, such as multiquark states, hybrid states, and glueballs, etc. The study of these exotic hadrons provides crucial insights into the non-perturbative behavior of QCD. Over the past few decades, significant advancements in high-energy physics experiments have led to the observation of a series of new hadronic states, such as the XYZ states [6–10] and hidden-charm pentaquark states [11, 12]. Since 2003, more than 60 new hadronic states have been discovered in high-energy physics experiments, and many more are expected to be found in the future. Exploring the hadronic structure underlying these experimental discoveries has emerged as a central focus in modern hadron physics research.

In 2020, the LHCb Collaboration reported the observation of a narrow structure, X(6900), with a global significance exceeding 5σ in the $J/\psi J/\psi$ invariant mass spectrum, as well as a broad structure in the range of 6.2 to 6.8 GeV, and a hint of another structure around 7.2 GeV in the di- J/ψ spectrum [13]. This marked the first experimental observation of distinct structures in the double- J/ψ mass spectrum, which is regarded as a major breakthrough in the exploration of hadron spectroscopy. Recently, the ATLAS and CMS Collaborations confirmed the existence of X(6900) in the $J/\psi J/\psi$ invariant mass spectrum with a significance far exceeding 5σ [14, 15]. In the same $J/\psi J/\psi$ channel, ATLAS also identified two additional structures, X(6400) and X(6600), while CMS observed X(6600) and X(7200) under two models, both with

and without considering the interference effects between resonances. Meanwhile, the ATLAS Collaboration reported signals of X(6900) and X(7200) in the $J/\psi\psi(2S)$ decay channel with a significance exceeding 4.7σ .

In recent years, fully heavy tetraquark states have attracted significant attention and have been extensively studied across various theoretical frameworks [16–77]. For instance, the authors of Ref. [75] conducted a systematic investigation of these states using a non-relativistic quark model grounded in lattice quantum chromodynamics. They addressed the four-body problem by applying the Gaussian expansion method and complex scaling technique, which revealed the presence of several narrow resonances across all examined tetraquark systems, each exhibiting strong decay widths of less than 30 MeV. In another study, Ref. [17] employed a relativized diquark model Hamiltonian to calculate the masses of ground state tetraquarks with quantum numbers $J^{PC} = 0^{++}$ and fully heavy baryons across various configurations, producing a comprehensive spectrum for all combinations of heavy quark flavors. Furthermore, the potential for molecular states in the $D^{(*)}\Xi_{cc}^{(*)}$ and $\bar{\Xi}_{cc}^{(*)}\Xi_{cc}^{(*)}$ systems was explored using heavy antiquark-diquark symmetry (HADS). This analysis predicted several meson-baryon and baryon-baryon molecules and suggested a potential connection between the states X(7200) and X(3872), as discussed in Ref. [74].

In addition, there are also quite a few papers that investigate fully heavy tetraquark states using QCD sum rules. In Ref. [69], the mass spectrum of the ground state and the first two excited states of fully-charm tetraquarks was studied using QCD sum rules and Regge trajectories. By incorporating experimental data, a self-consistent analysis was conducted, and the X(6600), X(6900), and X(7300) were tentatively assigned to tetraquark states with $J^{PC} = 0^{++}$ or 1^{-+} . Additionally, using the inverse Laplace transform sum rule, the masses of doubly-hidden scalar charmonium and bottomonium molecular states were calculated, yielding results consistent with the LHCb experimental observa-

*Electronic address: duancg@hebtu.edu.cn

†Electronic address: tangl@hebtu.edu.cn

‡Electronic address: qiaocf@ucas.ac.cn

tion range of 6.2-6.9 GeV [53]. Moreover, the mass spectra of S-wave and P-wave fully-charm $c\bar{c}c\bar{c}$ and fully-bottom $b\bar{b}\bar{b}\bar{b}$ tetraquark states in the $8_{[Q\bar{Q}]} \otimes 8_{[Q\bar{Q}]}$ color configuration have been systematically calculated using the moment QCD sum rule method [55], where the predicted masses for the fully-charm $c\bar{c}c\bar{c}$ tetraquark states are approximately 6.3-6.5 GeV for the S-wave channels and 7.0-7.2 GeV for the P-wave channels. Recently, Wan and Qiao proposed a nature hybrid interpretation for the structure of $X(6900)$, i.e. in $[\bar{3}_c]_{cc} \otimes [8_c]_G \otimes [\bar{3}_c]_{c\bar{c}}$ configuration with $J^{PC} = 0^{++}$; by using QCD sum rules, their results showed that the observed $X(6900)$ could be a gluonic tetracharm state, and some other structures may exist, e.g., one around 7.2 GeV in the tetracharm hybrid configuration and with $J^{PC} = 0^{-+}$ [56].

In our previous study, we systematically calculated the fully-heavy tetraquark states with various quantum numbers using QCD sum rules for the $[8_c]_{Q\bar{Q}} \otimes [8_c]_{Q\bar{Q}}$ type currents [76, 77]. In this work, we propose a new hybrid configuration: tetraquark hybrid state, i.e. $[8_c]_{[Q\bar{Q}]} \otimes [8_c]_{[G]} \otimes [8_c]_{[Q\bar{Q}]}$. The selection of this specific color configuration (e.g., $[8_c]_{Q\bar{Q}} \otimes [8_c]_G \otimes [8_c]_{Q\bar{Q}}$) is rooted in the SU(3) color symmetry constraints. To form a color-singlet hybrid state, the combined color representation of the quark-antiquark pairs and the valence gluon must satisfy: $(([8_c]_{Q\bar{Q}} \otimes [8_c]_{Q\bar{Q}}) \otimes [8_c]_G \rightarrow 1_c \oplus \dots)$. Only specific combinations (e.g., octet-octet-octet) can achieve an overall color singlet without triviality.

The inclusion of a valence gluon (g) fundamentally differentiates our configuration from the pure tetraquark system or the molecular state. On the one hand, the gluonic component introduces additional dynamical energy via non-Abelian interactions, leading to higher masses compared to pure $qq\bar{q}\bar{q}$ states, consistent with the established theoretical expectation for gluon mass contributions (e.g. $Q\bar{Q}g$ vs $Q\bar{Q}$) [78–81]. On the other hand, the valence gluon in our proposed tetraquark-gluon hybrid introduces distinct decay dynamics compared to pure tetraquark systems. This gluon-mediated modification alters selection rules and phase-space constraints, potentially suppressing or enhancing specific decay channels. Such decay pattern anomalies, if observed experimentally, would serve as direct diagnostic evidence for the hybrid nature of these states — a critical advantage over conventional tetraquark interpretations. Although lattice QCD and effective field theory studies of this specific configuration are currently absent, experimental anomalies strongly hint at its plausibility. For example, the proliferation of unclassified exotic states (e.g., P_c states [11, 12], $X(6600)$, $X(6900)$, $X(7200)/X(7300)$ [13–15], and so on) suggests the existence of unexplored hadronic configurations beyond conventional paradigms.

We perform the calculation of the spectrum of this structure within the framework of the QCD sum rules (QCDSR) [82]. Unlike phenomenological models, QCDSR is a theoretical framework based on QCD, which systematically incorporates non-perturbative effects and offers unique advantages in studying hadron properties involving non-perturbative QCD. It has achieved significant success in hadron spectroscopy research [76–104]. To establish QCDSR, the initial step in-

volves constructing suitable interpolating currents that correspond to the hadrons of interest. These currents are then used to create a two-point correlation function, which can be expressed in two ways: the QCD representation and the phenomenological representation. By setting these two representations equal to each other, QCDSR is formally established, enabling the extraction of the hadron's mass.

The remainder of this paper is structured as follows: Section II presents the primary formalism following the introduction. Section III details the numerical analysis and its results comprehensively. Finally, the concluding section discusses and summarizes the key findings.

II. FORMALISM

The QCD sum rules calculations rely on the correlator formed by two hadronic currents [82, 86, 88, 105, 106]. For scalar hadronic currents, the two-point correlation function is expressed as:

$$\Pi(q) = i \int d^4x e^{iq \cdot x} \langle 0 | T\{j(x), j^\dagger(0)\} | 0 \rangle. \quad (1)$$

The constructions of the tetracharm hybrid state with quantum numbers $J^{PC} = 0^{++}, 0^{-+}$ are described as follows:

$$j_A^{0^{++}} = g_s f^{abc} \left[\bar{Q}^j \gamma^\mu (t^a)_{jk} Q^k \right] G_{\mu\nu}^b \left[\bar{Q}^m \gamma^\nu (t^c)_{mn} Q^n \right], \quad (2)$$

$$j_B^{0^{++}} = g_s f^{abc} \left[\bar{Q}^j \gamma^\mu \gamma_5 (t^a)_{jk} Q^k \right] G_{\mu\nu}^b \left[\bar{Q}^m \gamma^\nu \gamma_5 (t^c)_{mn} Q^n \right], \quad (3)$$

$$j_A^{0^{-+}} = g_s f^{abc} \left[\bar{Q}^j \gamma^\mu (t^a)_{jk} Q^k \right] \tilde{G}_{\mu\nu}^b \left[\bar{Q}^m \gamma^\nu (t^c)_{mn} Q^n \right], \quad (4)$$

$$j_B^{0^{-+}} = g_s f^{abc} \left[\bar{Q}^j \gamma^\mu \gamma_5 (t^a)_{jk} Q^k \right] \tilde{G}_{\mu\nu}^b \left[\bar{Q}^m \gamma^\nu \gamma_5 (t^c)_{mn} Q^n \right]. \quad (5)$$

Here, g_s denotes the strong coupling constant, j, k, m, n represent color indices, taking values 1, 2, 3, a stands for color indices, taking values from 1 to 8, and μ, ν indicate Lorentz indices. $t^a = \frac{\lambda^a}{2}$, where λ^a are the Gell-Mann matrices, and t^a are the generators. The heavy quark field Q stands for either a charm quark or a bottom quark, while $G_{\mu\nu}^b$ signifies the gluon field strength tensor, and $\tilde{G}_{\mu\nu}^b = \frac{1}{2} \epsilon_{\mu\nu\alpha\beta} G^{b,\alpha\beta}$ denotes the dual gluon field strength tensor. It should be noted that the interpolating currents under discussion consist of two color-octet $Q\bar{Q}$ components along with one gluon, which are analyzed via QCD sum rules for the first time. The adopted interpolating currents for $J^{PC} = 0^{++}$ and 0^{-+} states adhere to the following configuration criteria, which require that (i) color-octet quark-antiquark pairs form S- or P-wave configurations, with their corresponding color-singlet-state quarkonium states being J/ψ (S-wave) or χ_{c1} (P-wave), respectively, and (ii) the interpolating currents be constructed by coupling them to $G_{\mu\nu}^a$ or $\tilde{G}_{\mu\nu}^a$, so as to ensure that these currents match the quantum numbers.

The principle of quark-hadron duality serves as the fundamental assumption for applying the QCD sum rule approach. Therefore, on the one hand, the correlation function $\Pi(q^2)$ can be calculated at the quark-gluon level using the Operator

Product Expansion (OPE); on the other hand, it can be expressed at the hadron level, where the hadrons coupling constant and mass are introduced. To calculate the spectral density on the OPE side, the “full” propagators $S_{jk}^Q(p)$ of a heavy quark ($Q = c$ or b) are utilized:

$$\begin{aligned} S_{jk}^Q(p) &= \frac{i\delta_{jk}(\not{p} + m_Q)}{p^2 - m_Q^2} - \frac{i}{4}g_s \frac{t_{jk}^a G_{\alpha\beta}^a}{(p^2 - m_Q^2)^2} [\sigma^{\alpha\beta}(\not{p} + m_Q) \\ &+ (\not{p} + m_Q)\sigma^{\alpha\beta}] - \frac{i}{4}g_s^2(t^a t^b)_{jk} G_{\alpha\beta}^a G_{\mu\nu}^b \frac{(\not{p} + m_Q)}{(p^2 - m_Q^2)^5} \\ &\times (f^{\alpha\beta\mu\nu} + f^{\alpha\mu\beta\nu} + f^{\alpha\mu\nu\beta})(\not{p} + m_Q) \\ &+ \frac{i\delta_{jk}}{48} \left\{ \frac{(\not{p} + m_Q)[\not{p}(p^2 - 3m_Q^2) + 2m_Q(2p^2 - m_Q^2)]}{(p^2 - m_Q^2)^6} \right. \\ &\left. \times (\not{p} + m_Q) \right\} \langle g_s^3 G^3 \rangle, \end{aligned} \quad (6)$$

the subscripts j and k denote the color indices of the heavy quark. Here, we define $f^{\alpha\beta\mu\nu} \equiv \gamma^\alpha(\not{p} + m_Q)\gamma^\beta(\not{p} + m_Q)\gamma^\mu(\not{p} + m_Q)\gamma^\nu$. For more detailed information regarding the discussed propagator, readers are encouraged to refer to references [83, 84, 86].

Thus, based on the dispersion relation, the correlation function $\Pi(q^2)$ at the quark-gluon level can be derived:

$$\Pi^{\text{OPE}}(q^2) = \int_{(4m_Q)^2}^{\infty} ds \frac{\rho^{\text{OPE}}(s)}{s - q^2}, \quad (7)$$

where $\rho^{\text{OPE}}(s) = \text{Im}[\Pi^{\text{OPE}}(s)]/\pi$ and

$$\rho^{\text{OPE}}(s) = \rho^{\text{pert}}(s) + \rho^{\langle GG \rangle}(s) + \rho^{\langle GGG \rangle}(s). \quad (8)$$

By using the Borel transformation to Eq. (7), we have

$$\Pi^{\text{OPE}}(M_B^2) = \int_{(4m_Q)^2}^{\infty} ds \rho^{\text{OPE}}(s) e^{-s/M_B^2}. \quad (9)$$

The typical leading order Feynman diagrams contributing to Eq. (9) for the tetracharm hybrid state are shown in Fig. 1. Diagram I represents the contribution from the perturbative part, Diagram II illustrates the two-gluon condensation, and Diagrams III and IV depict the three-gluon condensation. The full expression of the spectral density $\rho^{\text{OPE}}(s)$ is lengthy and will not be shown here.

From a phenomenological perspective, by isolating the ground state contribution of the tetracharm hybrid state, the correlation function $\Pi(q^2)$ can be expressed as a dispersion integral over the hadronic spectrum,

$$\Pi(q^2) = \frac{(\lambda_X)^2}{(M_X)^2 - q^2} + \frac{1}{\pi} \int_{s_0}^{\infty} ds \frac{\rho^h(s)}{s - q^2}, \quad (10)$$

where M_X is the mass of the the tetracharm hybrid state, and $\rho^h(s)$ is the spectral density that includes contributions from higher excited states and continuum states. s_0 denotes the threshold for the higher excited and continuum states. Based on the method detailed and explained in references [86, 106],

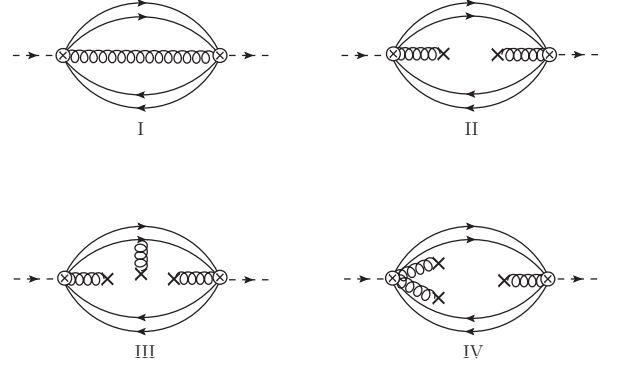


FIG. 1: The representative Feynman diagrams for a tetracharm hybrid state, where the permutation diagrams are implicitly accounted for, are shown. Diagrams I, II, III, and IV correspond to the contributions from the perturbative term, two-gluon condensate, and three-gluon condensate, respectively.

when calculating the phenomenological aspects of the QCD sum rules, a series of intermediate states must be inserted between the two tetracharm hybrid state interpolating currents. This summation encompasses all possible hadronic states that can be generated by the tetracharm hybrid state currents. The coupling constant λ_X is defined as follows:

$$\langle 0 | j^{0^{++}}(0) | X \rangle = \lambda_X, \quad (11)$$

where X is the lowest lying tetracharm hybrid state. By applying the Borel transformation to the phenomenological side (as described in Eq. (10)), and aligning it with Eq. (9), we obtain the main equation

$$(\lambda_X)^2 \exp\left(-\frac{M_X^2}{M_B^2}\right) = \int_{(4m_Q)^2}^{s_0} ds \rho^{\text{OPE}}(s) e^{-s/M_B^2}. \quad (12)$$

Finally, by differentiating Eq. (12) with respect to $\frac{1}{M_B^2}$, we derive the mass of the tetracharm hybrid state.

$$M_X(s_0, M_B^2) = \sqrt{-\frac{L_1(s_0, M_B^2)}{L_0(s_0, M_B^2)}}. \quad (13)$$

The moments L_0 and L_1 are defined as:

$$L_0(s_0, M_B^2) = \int_{(4m_Q)^2}^{s_0} ds \rho^{\text{OPE}}(s) e^{-s/M_B^2}, \quad (14)$$

$$L_1(s_0, M_B^2) = \frac{\partial}{\partial(M_B^2)^{-1}} L_0(s_0, M_B^2). \quad (15)$$

III. NUMERICAL ANALYSIS

The QCD sum rule expressions involve several input parameters, including the condensates and quark masses. These values have been determined in the literature [82, 86, 88, 105, 106]. For the numerical analysis, we take $m_c(m_c) = \bar{m}_c = (1.27 \pm 0.03)$ GeV and $m_b(m_b) = \bar{m}_b = (4.18 \pm 0.03)$ GeV,

$\langle g_s^2 G^2 \rangle = 0.88 \text{ GeV}^4$, $\langle g_s^3 G^3 \rangle = 0.045 \text{ GeV}^6$ where the $\overline{m}_c, \overline{m}_b$ are “running masses” of charm and bottom quarks in \overline{MS} scheme.

Additionally, the QCD sum rules introduce two extra parameters, M_B^2 and s_0 , corresponding to the Borel parameter and the threshold parameter, which must be determined following the standard procedures. Given a specific s_0 value, the Borel parameter M_B^2 is determined based on two fundamental conditions [82, 86, 105, 106]. To accurately extract the ground state properties of the tetracharm hybrid state, it is first necessary to ensure that the contribution from the continuum spectrum is secondary to the pole contribution (PC) [106, 107]. This condition can be expressed through a specific formula:

$$R_i^{\text{PC}}(s_0, M_B^2) = \frac{L_0(s_0, M_B^2)}{L_0(\infty, M_B^2)}, \quad (16)$$

where the subscript i represents different currents. Under this condition, the contributions from higher excited states and continuum states are significantly suppressed. This requirement can establish an upper threshold $(M_B^2)_{\max}$ for M_B^2 . The second condition concerns the convergence of the OPE. Specifically, it requires comparing the individual contributions with the total magnitude on the OPE side and selecting a reliable region for M_B^2 to maintain convergence, which will yield a lower bound $(M_B^2)_{\min}$ for M_B^2 . In practice, the degree of convergence can be expressed as the ratio of condensates to the total, as follows:

$$R_i^{\text{cond}}(s_0, M_B^2) = \frac{L_0^{\text{dim}}(s_0, M_B^2)}{L_0(s_0, M_B^2)}. \quad (17)$$

The superscript “dim” indicates the dimension of the relevant condensate in the OPE, as described in Eq. (14). Thus, for a given s_0 , the appropriate Borel window, i.e., the range between $(M_B^2)_{\min}$ and $(M_B^2)_{\max}$, has been determined. In this work, to verify whether the OPE convergence criterion is satisfied, we first ensure that the contribution from the highest-order condensate $\langle G^3 \rangle$ does not exceed 10% of the total OPE contribution.

Certainly, it is necessary to impose a constraint on the value of s_0 , specifically requiring that the mass of the tetracharm hybrid state M_X exhibits minimal dependence on the parameter s_0 . We employed a method similar to that described in references [108–110] to analyze and accurately determine the appropriate continuum threshold s_0 . Note that the relationship between s_0 and the ground state mass is given by $\sqrt{s_0} \approx (M_X + \delta) \text{ GeV}$, where δ ranges from 0.40 to 0.80 GeV. Therefore, in numerical evaluations, exploring different values of $\sqrt{s_0}$ is crucial to meeting this criterion. Among these values, we need to select the one that produces the optimal window for the Borel parameter M_B^2 . In other words, within the optimal window, the mass of the tetraquark hybrid M_X is, to some extent, independent of the Borel parameter M_B^2 . Thus, the value of $\sqrt{s_0}$ corresponding to the optimal mass curve will be taken as the central value. In practical applications, we can vary $\sqrt{s_0}$ by 0.2 GeV in numerical calculations, which sets the upper and lower bounds for $\sqrt{s_0}$ and helps determine its uncertainty.

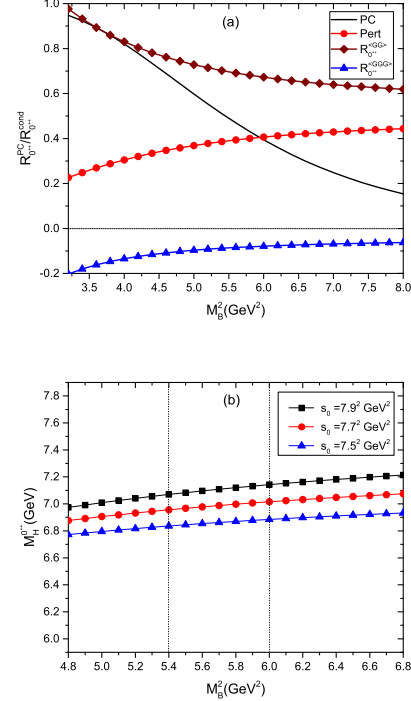


FIG. 2: Figures of the current $j_A^{0^{++}}$. (a) The pole contribution ratio $R_{0^{++}}^{\text{PC}}$ and the OPE convergence ratio $R_{0^{++}}^{\text{cond}}$ as functions of the Borel parameter M_B^2 for the central value of s_0 ; (b) the mass $M_X^{0^{++}}$ varies with M_B^2 , with the selected s_0 values being $s_0 = 7.50^2 \text{ GeV}^2$, 7.70^2 GeV^2 , and 7.90^2 GeV^2 from bottom to top. Two vertical lines indicate the upper and lower limits of the effective Borel window with s_0 as the central value.

For the tetracharm hybrid state represented by the current $j_A^{0^{++}}(x)$, characterized by $J^{PC} = 0^{++}$, we present in Fig. 2(a) the variation of two ratios, $R_{0^{++},A}^{\text{PC}}$ and $R_{0^{++},A}^{\text{cond}}$, as functions of the Borel parameter M_B^2 , with a selected $s_0 = 7.70^2 \text{ GeV}^2$. In Fig. 2(b), we depict the mass relationship with M_B^2 for different s_0 values, also including two lines indicating the upper and lower limits of the effective Borel window under the central s_0 value. The selection of M_B^2 and s_0 complies with the three criteria elaborated earlier. For case $j_B^{0^{++}}(x)$, a similar numerical analysis is conducted, and specific results are presented in Fig. 3. Notably, the three-gluon condensate contributions for currents $j_A^{0^{++}}$ and $j_B^{0^{++}}$ remain below 10% within each Borel window, satisfying the above-mentioned OPE truncation criterion established, and validating the truncation scheme [78–81].

For currents (3) and (4), we could not obtain a positive spectral density function $\rho_B^{0^{++}}$ and $\rho_A^{0^{++}}$, indicating that the current structures in Eqs. (3) and (4) do not support the respective tetracharm hybrid states. Therefore, the article only presents numerical curves for the currents $j_A^{0^{++}}$ and $j_B^{0^{++}}$. The resulting windows of Borel parameter M_B^2 , continuum thresholds s_0 , pole contributions, masses, and pole residues are succinctly

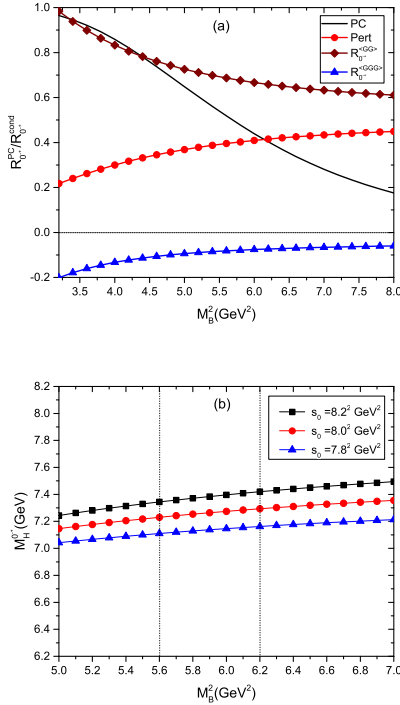


FIG. 3: The same caption as in Fig. 2, but for the current j_B^{0-+} .

J^{PC}	$M_B^2 (\text{GeV}^2)$	$\sqrt{s_0} (\text{GeV})$	PC	$M_X (\text{GeV})$	$\lambda_X (10^{-1} \text{GeV}^5)$
j_A^{0++}	$5.40 - 6.00$	7.70 ± 0.20	$(50 - 40)\%$	$6.98_{-0.14}^{+0.16}$	$0.99_{-0.09}^{+0.08}$
j_B^{0-+}	$5.60 - 6.20$	8.00 ± 0.20	$(50 - 40)\%$	$7.26_{-0.15}^{+0.16}$	$0.86_{-0.08}^{+0.07}$

TABLE I: The ranges of Borel parameter M_B^2 , the threshold parameter s_0 , the pole contributions (PC), masses, and the ground state pole residues for currents j_A^{0++} and j_B^{0-+} .

listed in Table I. As seen in the table, the dominance of the pole contribution in the phenomenological analysis is well fulfilled within the appropriate Borel window. Within this window, the mass curves display a stable plateau. The central values are consistent with the most stable results concerning M_B^2 , while the error ranges arise from variations in the condensates, quark masses, and the parameters s_0 and M_B^2 .

We provide Table II to compare our mass predictions and experimental observations.

	This work	LHCb [13]	CMS [14]	ATLAS [15]
j_A^{0++}	6980_{-140}^{+160}	6905 ± 11	6927 ± 9	6870 ± 30
j_B^{0-+}	7260_{-150}^{+160}	—	7287 ± 19	7220 ± 30

TABLE II: A comparison between the theoretically predicted masses (in unit of MeV) in this study and the results reported by the LHCb, CMS, and ATLAS experimental collaborations.

Similarly, by replacing the charm quark in theoretical calculations and numerical analysis with the bottom quark, we can predict the masses of tetrabottom hybrid states to be $19.30_{-0.17}^{+0.16}$ and $19.50_{-0.17}^{+0.17}$, respectively.

IV. CONCLUSIONS

In this study, we propose a novel hadronic structure composed of two color-octet $\bar{Q}Q$ components and a color-octet gluon ($[8_c]_{Q\bar{Q}} \otimes [8_c]_G \otimes [8_c]_{Q\bar{Q}}$). We investigate the tetracharm hybrid currents with quantum numbers 0^{++} and 0^{-+} . The results reveal that the mass of the tetracharm hybrid state corresponding to the 0^{++} current is $6.98_{-0.14}^{+0.16}$ GeV, while the mass associated with the 0^{-+} current is $7.26_{-0.15}^{+0.16}$ GeV. Our analysis suggests that the newly observed states X(6900) and X(7200) correspond to the proposed hadronic structure with 0^{++} and 0^{-+} , respectively, or, at least they may possess significant tetracharm hybrid components.

Table II provides a systematic comparison between our QCD sum rule calculations for the $cc\bar{c}\bar{c}G$ hybrid masses and experimentally measured masses of X(6900) and X(7200) reported by the LHCb, ATLAS, and CMS collaborations. Both theoretical uncertainties and experimental errors are quantified in the table. Crucially, conventional theoretical frameworks (e.g., potential models, lattice QCD) have exclusively addressed tetraquark systems lacking explicit valence gluons — a fundamental distinction from our tetracharm-gluon hybrid configuration. To date, no rigorous predictions for tetracharm-gluon hybrids corresponding to our proposed $cc\bar{c}\bar{c}G$ (color-octet-octet-octet) states have been proposed in the literature, underscoring the novelty of this work.

Furthermore, we extended our analysis to the bottom sector and obtained the masses of the corresponding tetrabottom hybrid states with quantum numbers 0^{++} and 0^{-+} as $19.30_{-0.17}^{+0.16}$ GeV and $19.50_{-0.17}^{+0.17}$ GeV, respectively. These states may be observed in future experimental studies.

Acknowledgments

This work is supported by the National Natural Science Foundation of China (NSFC) under Grant No. 11975090, 12475087 and 12235008; the Natural Science Foundation of Hebei Province under Grant No. A2023205038 and S&T Program of Hebei (Grant No. 22567617H).

-
- [1] M. Gell-Mann, Phys. Lett. **8**, 214-215 (1964).
- [2] G. Zweig, Version 1. CERN-TH-401, CERN, Geneva, 1964
- [3] D. J. Gross and F. Wilczek, Phys. Rev. Lett. **30**, 1343-1346 (1973)
- [4] H. D. Politzer, Phys. Rev. Lett. **30**, 1346-1349 (1973)
- [5] K. G. Wilson, Phys. Rev. D **10**, 2445-2459 (1974)
- [6] S. K. Choi *et al.* [Belle], Phys. Rev. Lett. **91**, 262001 (2003)
- [7] B. Aubert *et al.* [BaBar], Phys. Rev. Lett. **95**, 142001 (2005)
- [8] A. Bondar *et al.* [Belle], Phys. Rev. Lett. **108**, 122001 (2012)
- [9] M. Ablikim *et al.* [BESIII], Phys. Rev. Lett. **110**, 252001 (2013)
- [10] Z. Q. Liu *et al.* [Belle], Phys. Rev. Lett. **110**, 252002 (2013) [erratum: Phys. Rev. Lett. **111**, 019901 (2013)]
- [11] R. Aaij *et al.* [LHCb], Phys. Rev. Lett. **115**, 072001 (2015)
- [12] R. Aaij *et al.* [LHCb], Phys. Rev. Lett. **122**, 222001 (2019)
- [13] R. Aaij *et al.* [LHCb], Sci. Bull. **65**, 1983-1993 (2020) [arXiv:2006.16957 [hep-ex]].
- [14] A. Hayrapetyan *et al.* [CMS], Phys. Rev. Lett. **132**, 111901 (2024).
- [15] G. Aad *et al.* [ATLAS], Phys. Rev. Lett. **131**, 151902 (2023).
- [16] M. N. Anwar, J. Ferretti, F. K. Guo, E. Santopinto and B. S. Zou, Eur. Phys. J. C **78**, 647 (2018) [arXiv:1710.02540 [hep-ph]].
- [17] M. A. Bedolla, J. Ferretti, C. D. Roberts and E. Santopinto, Eur. Phys. J. C **80**, 1004 (2020) [arXiv:1911.00960 [hep-ph]].
- [18] R. J. Lloyd and J. P. Vary, Phys. Rev. D **70**, 014009 (2004) [arXiv:hep-ph/0311179 [hep-ph]].
- [19] N. Barnea, J. Vijande and A. Valcarce, Phys. Rev. D **73**, 054004 (2006) [arXiv:hep-ph/0604010 [hep-ph]].
- [20] V. R. Debastiani and F. S. Navarra, Chin. Phys. C **43**, 013105 (2019) [arXiv:1706.07553 [hep-ph]].
- [21] J. Wu, Y. R. Liu, K. Chen, X. Liu and S. L. Zhu, Phys. Rev. D **97**, 094015 (2018) [arXiv:1605.01134 [hep-ph]].
- [22] G. J. Wang, L. Meng and S. L. Zhu, Phys. Rev. D **100**, 096013 (2019) [arXiv:1907.05177 [hep-ph]].
- [23] M. S. Liu, Q. F. Lü, X. H. Zhong and Q. Zhao, Phys. Rev. D **100**, 016006 (2019) [arXiv:1901.02564 [hep-ph]].
- [24] R. N. Faustov, V. O. Galkin and E. M. Savchenko, Phys. Rev. D **102**, 114030 (2020) [arXiv:2009.13237 [hep-ph]].
- [25] Q. F. Lü, D. Y. Chen and Y. B. Dong, Eur. Phys. J. C **80**, 871 (2020) [arXiv:2006.14445 [hep-ph]].
- [26] W. Heupel, G. Eichmann and C. S. Fischer, Phys. Lett. B **718**, 545-549 (2012) [arXiv:1206.5129 [hep-ph]].
- [27] X. Z. Weng, X. L. Chen, W. Z. Deng and S. L. Zhu, Phys. Rev. D **103**, 034001 (2021) [arXiv:2010.05163 [hep-ph]].
- [28] A. V. Berezhnoy, A. V. Luchinsky and A. A. Novoselov, Phys. Rev. D **86**, 034004 (2012) [arXiv:1111.1867 [hep-ph]].
- [29] M. Karliner, S. Nussinov and J. L. Rosner, Phys. Rev. D **95**, 034011 (2017) [arXiv:1611.00348 [hep-ph]].
- [30] A. V. Berezhnoy, A. K. Likhoded, A. V. Luchinsky and A. A. Novoselov, Phys. Rev. D **84**, 094023 (2011) [arXiv:1101.5881 [hep-ph]].
- [31] F. Feng, Y. Huang, Y. Jia, W. L. Sang, X. Xiong and J. Y. Zhang, Phys. Rev. D **106**, 114029 (2022) [arXiv:2009.08450 [hep-ph]].
- [32] H. F. Zhang and Y. Q. Ma, [arXiv:2009.08376 [hep-ph]].
- [33] M. Karliner and J. L. Rosner, Phys. Rev. D **102**, 114039 (2020) [arXiv:2009.04429 [hep-ph]].
- [34] J. Z. Wang, D. Y. Chen, X. Liu and T. Matsuki, Phys. Rev. D **103**, 071503 (2021) [arXiv:2008.07430 [hep-ph]].
- [35] J. F. Giron and R. F. Lebed, Phys. Rev. D **102**, 074003 (2020) [arXiv:2008.01631 [hep-ph]].
- [36] K. T. Chao and S. L. Zhu, Sci. Bull. **65**, 1952-1953 (2020) [arXiv:2008.07670 [hep-ph]].
- [37] L. Maiani, Sci. Bull. **65**, 1949-1951 (2020) [arXiv:2008.01637 [hep-ph]].
- [38] J. M. Richard, Sci. Bull. **65**, 1954-1955 (2020) [arXiv:2008.01962 [hep-ph]].
- [39] R. Zhu, Nucl. Phys. B **966**, 115393 (2021) [arXiv:2010.09082 [hep-ph]].
- [40] Z. H. Guo and J. A. Oller, Phys. Rev. D **103**, 034024 (2021) [arXiv:2011.00978 [hep-ph]].
- [41] R. Maciąła, W. Schäfer and A. Szczurek, Phys. Lett. B **812**, 136010 (2021) [arXiv:2009.02100 [hep-ph]].
- [42] J. W. Zhu, X. D. Guo, R. Y. Zhang, W. G. Ma and X. Q. Li, [arXiv:2011.07799 [hep-ph]].
- [43] G. Eichmann, C. S. Fischer, W. Heupel, N. Santowsky and P. C. Wallbott, Few Body Syst. **61**, 38 (2020) [arXiv:2008.10240 [hep-ph]].
- [44] C. Gong, M. C. Du, Q. Zhao, X. H. Zhong and B. Zhou, Phys. Lett. B **824**, 136794 (2022) [arXiv:2011.11374 [hep-ph]].
- [45] C. Becchi, J. Ferretti, A. Giachino, L. Maiani and E. Santopinto, Phys. Lett. B **811**, 135952 (2020).
- [46] X. K. Dong, V. Baru, F. K. Guo, C. Hanhart and A. Nefediev, Phys. Rev. Lett. **126**, 132001 (2021) [erratum: Phys. Rev. Lett. **127**, 119901 (2021)] [arXiv:2009.07795 [hep-ph]].
- [47] W. Chen, H. X. Chen, X. Liu, T. G. Steele and S. L. Zhu, Phys. Lett. B **773**, 247-251 (2017) [arXiv:1605.01647 [hep-ph]].
- [48] Z. G. Wang, Eur. Phys. J. C **77**, 432 (2017) [arXiv:1701.04285 [hep-ph]].
- [49] W. Chen, H. X. Chen, X. Liu, T. G. Steele and S. L. Zhu, EPJ Web Conf. **182**, 02028 (2018) [arXiv:1803.02522 [hep-ph]].
- [50] Z. G. Wang and Z. Y. Di, Acta Phys. Polon. B **50**, 1335 (2019) [arXiv:1807.08520 [hep-ph]].
- [51] J. R. Zhang, Phys. Rev. D **103**, 014018 (2021).
- [52] Z. G. Wang, Int. J. Mod. Phys. A **36**, 2150014 (2021).
- [53] R. M. Albuquerque, S. Narison, A. Rabemananjara, D. Rabettiarivony and G. Randriamananjaka, Phys. Rev. D **102**, 094001 (2020) [arXiv:2008.01569 [hep-ph]].
- [54] H. X. Chen, W. Chen, X. Liu and S. L. Zhu, Sci. Bull. **65**, 1994-2000 (2020) [arXiv:2006.16027 [hep-ph]].
- [55] Q. N. Wang, Z. Y. Yang and W. Chen, Phys. Rev. D **104**, 114037 (2021) [arXiv:2109.08091 [hep-ph]].
- [56] B. D. Wan and C. F. Qiao, Phys. Lett. B **817**, 136339 (2021) [arXiv:2012.00454 [hep-ph]].
- [57] S. S. Agaev, K. Azizi, B. Barsbay and H. Sundu, Phys. Lett. B **844**, 138089 (2023) [arXiv:2304.03244 [hep-ph]].
- [58] S. S. Agaev, K. Azizi, B. Barsbay and H. Sundu, Nucl. Phys. A **1041**, 122768 (2024) [arXiv:2304.09943 [hep-ph]].
- [59] S. S. Agaev, K. Azizi, B. Barsbay and H. Sundu, Eur. Phys. J. Plus **138**, 935 (2023) [arXiv:2305.03696 [hep-ph]].
- [60] S. S. Agaev, K. Azizi, B. Barsbay and H. Sundu, Eur. Phys. J. C **83**, 994 (2023) [arXiv:2307.01857 [hep-ph]].
- [61] S. S. Agaev, K. Azizi, B. Barsbay and H. Sundu, Phys. Rev. D **109**, 014006 (2024) [arXiv:2310.10384 [hep-ph]].
- [62] X. Jin, Y. Xue, H. Huang and J. Ping, Eur. Phys. J. C **80**, 1083 (2020) [arXiv:2006.13745 [hep-ph]].
- [63] J. Zhao, S. Shi and P. Zhuang, Phys. Rev. D **102**, 114001 (2020) [arXiv:2009.10319 [hep-ph]].
- [64] Z. G. Wang, Chin. Phys. C **44**, 113106 (2020) [arXiv:2006.13028 [hep-ph]].
- [65] G. J. Wang, L. Meng, M. Oka and S. L. Zhu, Phys. Rev. D

- 104**, 036016 (2021) [arXiv:2105.13109 [hep-ph]].
- [66] F. X. Liu, M. S. Liu, X. H. Zhong and Q. Zhao, Phys. Rev. D **104**, 116029 (2021) [arXiv:2110.09052 [hep-ph]].
- [67] H. Mutuk, Eur. Phys. J. C **81**, 367 (2021) [arXiv:2104.11823 [hep-ph]].
- [68] X. K. Dong, V. Baru, F. K. Guo, C. Hanhart, A. Nefediev and B. S. Zou, Sci. Bull. **66**, 2462-2470 (2021).
- [69] Z. G. Wang, Nucl. Phys. B **985**, 115983 (2022) [arXiv:2207.08059 [hep-ph]].
- [70] J. Z. Wang and X. Liu, Phys. Rev. D **106**, 054015 (2022)
- [71] C. Gong, M. C. Du and Q. Zhao, Phys. Rev. D **106**, 054011 (2022) [arXiv:2206.13867 [hep-ph]].
- [72] G. L. Yu, Z. Y. Li, Z. G. Wang, J. Lu and M. Yan, Eur. Phys. J. C **83**, 416 (2023) [arXiv:2212.14339 [hep-ph]].
- [73] Z. G. Wang, Phys. Lett. B **819**, 136464 (2021) [arXiv:2104.03103 [hep-ph]].
- [74] M. Z. Liu and L. S. Geng, Eur. Phys. J. C **81**, 179 (2021) [arXiv:2012.05096 [hep-ph]].
- [75] G. Yang, J. Ping and J. Segovia, Phys. Rev. D **104**, 014006 (2021) [arXiv:2104.08814 [hep-ph]].
- [76] B. C. Yang, L. Tang and C. F. Qiao, Eur. Phys. J. C **81**, 324 (2021).
- [77] C. M. Tang, C. G. Duan and L. Tang, Eur. Phys. J. C **84**, 743 (2024) [arXiv:2405.05042 [hep-ph]].
- [78] C. F. Qiao, L. Tang, G. Hao and X. Q. Li, J. Phys. G **39**, 015005 (2012) [arXiv:1012.2614 [hep-ph]].
- [79] W. Chen, R. T. Kleiv, T. G. Steele, B. Bulthuis, D. Harnett, J. Ho, T. Richards and S. L. Zhu, JHEP **09**, 019 (2013) [arXiv:1304.4522 [hep-ph]].
- [80] W. Chen, T. G. Steele and S. L. Zhu, J. Phys. G **41**, 025003 (2014) [arXiv:1306.3486 [hep-ph]].
- [81] Z. G. Wang, [arXiv:2412.11038 [hep-ph]].
- [82] M. A. Shifman, A. I. Vainshtein and V. I. Zakharov, Nucl. Phys. B **147**, 385-447 (1979)
- [83] R. M. Albuquerque, arXiv:1306.4671 [hep-ph].
- [84] Z. G. Wang and T. Huang, Phys. Rev. D **89**, 054019 (2014).
- [85] J. Govaerts, L. J. Reinders, H. R. Rubinstein and J. Weyers, Nucl. Phys. B **258**, 215-229 (1985).
- [86] L. J. Reinders, H. Rubinstein and S. Yazaki, Phys. Rept. **127**, 1 (1985).
- [87] P. Colangelo and A. Khodjamirian, in *At the frontier of particle physics / Handbook of QCD*, edited by M. Shifman (World Scientific, Singapore, 2001), arXiv:hep-ph/0010175.
- [88] S. Narison, World Sci. Lect. Notes Phys. **26** 1 (1989).
- [89] C. M. Tang, Y. C. Zhao and L. Tang, Phys. Rev. D **105**, 114004 (2022).
- [90] C. F. Qiao and L. Tang, Phys. Rev. Lett. **113**, 221601 (2014).
- [91] L. Tang and C. F. Qiao, Nucl. Phys. B **904**, 282 (2016).
- [92] L. Tang, B. D. Wan, K. Maltman and C. F. Qiao, Phys. Rev. D **101**, 094032 (2020).
- [93] B. D. Wan, L. Tang and C. F. Qiao, Eur. Phys. J. C **80**, 121 (2020).
- [94] B. D. Wan and C. F. Qiao, Nucl. Phys. B **968**, 115450 (2021).
- [95] S. N. Li and L. Tang, [arXiv:2404.11145 [hep-ph]].
- [96] B. D. Wan, S. Q. Zhang and C. F. Qiao, Phys. Rev. D **105**, 014016 (2022).
- [97] Y. C. Zhao, C. M. Tang and L. Tang, Eur. Phys. J. C **83**, 654 (2023).
- [98] B. D. Wan, S. Q. Zhang and C. F. Qiao, Phys. Rev. D **106**, 074003 (2022).
- [99] S. Q. Zhang, B. D. Wan, L. Tang and C. F. Qiao, Phys. Rev. D **106**, 074010 (2022).
- [100] B. D. Wan and C. F. Qiao, [arXiv:2208.14042 [hep-ph]].
- [101] F. H. Yin, W. Y. Tian, L. Tang and Z. H. Guo, Eur. Phys. J. C **81**, 818 (2021).
- [102] B. D. Wan, [arXiv:2311.13161 [hep-ph]].
- [103] B. D. Wan, Nucl. Phys. B **1004**, 116538 (2024).
- [104] B. D. Wan and H. T. Xu, Chin. Phys. C **44**, 093105 (2024).
- [105] M. A. Shifman, A. I. Vainshtein and V. I. Zakharov, Nucl. Phys. B **147**, 448-518 (1979).
- [106] P. Colangelo and A. Khodjamirian, [arXiv:hep-ph/0010175 [hep-ph]].
- [107] R. D. Matheus, S. Narison, M. Nielsen and J. M. Richard, Phys. Rev. D **75**, 014005 (2007) [arXiv:hep-ph/0608297 [hep-ph]].
- [108] S. I. Finazzo, M. Nielsen and X. Liu, Phys. Lett. B **701**, 101-106 (2011) [arXiv:1102.2347 [hep-ph]].
- [109] C. F. Qiao and L. Tang, Eur. Phys. J. C **74**, 3122 (2014) [arXiv:1307.6654 [hep-ph]].
- [110] C. F. Qiao and L. Tang, Eur. Phys. J. C **74**, 2810 (2014) [arXiv:1308.3439 [hep-ph]].

Appendix

The currents $j_A^{0^{++}}$ and $j_B^{0^{-+}}$ are represented in the spectral density $\rho^{\text{OPE}}(s)$ as follows:

$$\begin{aligned}\rho_{0^{++},A}^{\text{pert}}(s) &= \frac{g_s^2}{2^{12} \times 5\pi^8} \int_{x_i}^{x_f} dx \int_{y_i}^{y_f} dy \int_{z_i}^{z_f} dz \left\{ F_{xyz}^6 (1 - x - y - z) xyz \right\} \\ &\quad - \frac{3g_s^2}{2^{12} \times 5\pi^8} \int_{x_i}^{x_f} dx \int_{y_i}^{y_f} dy \int_{z_i}^{z_f} dz \int_{\omega_i}^{\omega_f} d\omega \left\{ F_{xyz\omega}^5 m_Q^2 (xy + z\omega) \right\},\end{aligned}\quad (18)$$

$$\begin{aligned}\rho_{0^{++},A}^{\langle GG \rangle}(s) &= \frac{\langle g_s^2 GG \rangle}{2^{11} \times \pi^6} \int_{x_i}^{x_f} dx \int_{y_i}^{y_f} dy \int_{z_i}^{z_f} dz \left\{ F_{xyz}^2 m_Q^2 (6m_Q^2 - (2F_{xyz} - 3s)(x(y - z) \right. \\ &\quad \left. - z(y + z - 1))) \right\},\end{aligned}\quad (19)$$

$$\begin{aligned}\rho_{0^{++},A}^{\langle GGG \rangle}(s) &= \frac{\langle g_s^3 GGG \rangle}{2^{12} \times \pi^6} \int_{x_i}^{x_f} dx \int_{y_i}^{y_f} dy \int_{z_i}^{z_f} dz \frac{1}{xyz(x + y + z - 1)} \left\{ 3F_{xyz} m_Q^2 (x^2(y + z) \right. \\ &\quad + x(y^2 + y(2z - 1) + (z - 1)z) + yz(y + z - 1))(2m_Q^2 - (F_{xyz} - s)(x(y - z) \right. \\ &\quad - z(y + z - 1))) - 6(4F_{xyz}^3 xyz(x + y + z - 1) + 3F_{xyz}^2 (m_Q^2(x(y - z) \right. \\ &\quad - z(y + z - 1)) - 6sxyz(x + y + z - 1)) - 2F_{xyz}(m_Q^4 + 3m_Q^2 s(x(y - z) \right. \\ &\quad - z(y + z - 1)) - 6s^2 xyz(x + y + z - 1)) - s(-m_Q^4 + m_Q^2 s(x(z - y) \right. \\ &\quad \left. + z(y + z - 1)) + s^2 xyz(x + y + z - 1))) \right\},\end{aligned}\quad (20)$$

$$\begin{aligned}\rho_{0^{-+},B}^{\text{pert}}(s) &= \frac{g_s^2}{2^{12} \times 5\pi^8} \int_{x_i}^{x_f} dx \int_{y_i}^{y_f} dy \int_{z_i}^{z_f} dz \left\{ F_{xyz}^6 (1 - x - y - z) xyz \right\} \\ &\quad + \frac{3g_s^2}{2^{12} \times 5\pi^8} \int_{x_i}^{x_f} dx \int_{y_i}^{y_f} dy \int_{z_i}^{z_f} dz \int_{\omega_i}^{\omega_f} d\omega \left\{ F_{xyz\omega}^5 m_Q^2 (xy + z\omega) \right\},\end{aligned}\quad (21)$$

$$\begin{aligned}\rho_{0^{-+},B}^{\langle GG \rangle}(s) &= \frac{\langle g_s^2 GG \rangle}{2^{11} \times \pi^6} \int_{x_i}^{x_f} dx \int_{y_i}^{y_f} dy \int_{z_i}^{z_f} dz \left\{ -F_{xyz}^2 m_Q^2 (6m_Q^2 + (2F_{xyz} - 3s)(x(y - z) \right. \\ &\quad \left. - z(y + z - 1))) \right\},\end{aligned}\quad (22)$$

$$\begin{aligned}\rho_{0^{-+},B}^{\langle GGG \rangle}(s) &= \frac{\langle g_s^3 GGG \rangle}{2^{12} \times \pi^6} \int_{x_i}^{x_f} dx \int_{y_i}^{y_f} dy \int_{z_i}^{z_f} dz - \frac{1}{xyz(x + y + z - 1)} \left\{ 3F_{xyz} m_Q^2 (x^2(y + z) \right. \\ &\quad + x(y^2 + y(2z - 1) + (z - 1)z) + yz(y + z - 1))(2m_Q^2 + (F_{xyz} - s)(x(y - z) \right. \\ &\quad - z(y + z - 1))) - 6(4F_{xyz}^3 xyz(x + y + z - 1) - 18F_{xyz}^2 sxyz(x + y + z - 1) \right. \\ &\quad \left. + 2F_{xyz}(m_Q^4 + 6s^2 xyz(x + y + z - 1)) - s(m_Q^4 + s^2 xyz(x + y + z - 1))) \right\},\end{aligned}\quad (23)$$

Here, we use the following definition:

$$F_{xyz} = m_Q^2 f_{xyz} - s, \quad (24)$$

$$F_{xyz\omega} = \left(\frac{1}{x} + \frac{1}{y} + \frac{1}{z} + \frac{1}{w} \right) m_Q^2 - s, \quad (25)$$

$$x_{f/i} = \left[\left(1 - \frac{8m_Q^2}{s} \right) \pm \sqrt{\left(1 - \frac{8m_Q^2}{s} \right)^2 - \frac{4m_Q^2}{s}} \right] / 2, \quad (26)$$

$$y_{f/i} = \left[1 + 2x + \frac{3sx^2}{m_Q^2 - sx} \pm \sqrt{\frac{[m_Q^2 + sx(x-1)][(8x+1)m_Q^2 + sx(x-1)]}{(m_Q^2 - sx)^2}} \right] / 2, \quad (27)$$

$$z_{f/i} = \left[(1-x-y) \pm \sqrt{\frac{(x+y-1)[m_Q^2(x+y-(x-y)^2) + sxy(x+y-1)]}{sxy - (x+y)m_Q^2}} \right] / 2, \quad (28)$$

$$w_- = \frac{xyzm_Q^2}{sxyz - (xy + yz + xz)m_Q^2}, w_+ = 1 - x - y - z. \quad (29)$$